

AN IMPROVED TRANSIENT QUASI-ANALYSIS METHOD FOR OFFSET REFLECTOR IN IMPULSE RADIATING ANTENNA APPLICATIONS

C. Wu¹, F. Yang^{1,*}, J. Diao¹, J. OuYang¹, and H. Zhou²

¹School of Electronic Engineering, University of Electronic Science and Technology of China (UESTC), Chengdu 610054, China

²Institute of Applied Physical and Computational Mathematics, China

Abstract—A transient quasi-analytic method is improved to analyze the offset reflector for impulse radiating antenna (IRA) applications. Physical optic (PO) approximation and analytic time transform (ATT) are utilized to investigate the time domain (TD) radiating characteristics of the offset reflector. With the appropriate coordinate transformation, the TD far-field integral problem can be simplified to one dimensional angular integral which is independent of the reflector's size. In addition, the Fast Fourier Transform (FFT) of impulse responses is compared to the direct frequency domain result, and good agreement is obtained.

1. INTRODUCTION

The impulse radiating antenna (IRA) firstly proposed by Baum et al. is a promising issue for antenna engineers for the past decades [1–3]. Due to its frequency independent characteristics, parabolic reflectors are good candidates for IRA applications. However, the blocking effects caused by the feed are inevitable in the centered IRAs. To avoid this problem, the offset design is used in [4]. In order to analyze the time domain (TD) radiation characteristics, direct transient analysis of offset IRAs is essential.

Among several methodologies developed for transient analysis, the most widely used are full-wave methods and high-frequency approximation approaches. For full-wave methods, finite-difference time-domain (FDTD) [5] and time domain integral equation (TDIE) [6] are always employed. A polarimetric scattering from two-dimensional

Received 12 November 2011, Accepted 22 December 2011, Scheduled 24 December 2011

* Corresponding author: Feng Yang (yangf@uestc.edu.cn).

rough surface is presented by FDTD algorithm in [5], and wire structures are analyzed using TDIE in [6]. These methods provide a controlled accuracy, but they are time-consuming and require enormous memory for offset reflector analysis. Nevertheless, these shortcomings can be avoided with high frequency approximation approaches such as time domain physical optics (TD-PO) [7], time domain physical theory of diffraction (TD-PTD) [8], time domain uniform geometrical theory of diffraction (TD-UTD) [9] and ray tracing methods [10]. While the main problem of TD-PO is that the two-dimension TD far-field numerical integral is still time-consuming. A quasi-analytical solution for parabolas of revolution based on TD-PO can reduce the computation time dramatically. However, it cannot be directly used in offset reflector analysis [11–12].

In this paper, the method in [11] is further improved to calculate the offset reflector with a planar edge. Time domain Gaussian beam (TD-GB) is chosen as the feed. The offset reflector can be approximated by a second order surface. PO approximation and analytic time transform (ATT) are utilized to investigate TD radiating characteristics of the offset reflector. With the appropriate coordinate transformation, the TD far-field integral problem can be simplified to one dimensional angular integral which is independent of the reflector's size. This quasi-analysis method is highly efficient and can avoid the ray-caustic problem encountered in ray tracing methods. Finally, the Fast Fourier Transform (FFT) of impulse responses are also compared to the direct frequency domain (FD) result and good agreement is achieved. It is a promising approach for the transient analysis of offset IRAs.

2. DESCRIPTION OF TD-GB IN FREE SPACE

According to [11] the analytical step response of TD-GB in free space is expressed as

$$\vec{h}_+^u(\vec{r}_i, t) = \vec{H}_i^\delta(0) \sqrt{\frac{Det[Q^i(z_i)]}{Det[Q^i(0)]}} U_+ \left[t - \frac{q(\vec{r}_i)}{v} \right] \quad (1)$$

where $\vec{H}_i^\delta(0)$ is the GB's value at $(0, 0, 0)$, $Q^i(z_i)$ is the GB's complex curvature matrix at $(0, 0, z_i)$, $Det[A]$ stands for the determinant of a matrix A , and v is the speed of light, $U_+[t]$ can be expressed as [13]

$$U_+[t] = 1 + \frac{j}{\pi} (\ln t + \gamma) \quad (2)$$

and $\gamma = 0.5772$ is Euler's constant.

$$q(\vec{r}_i) = z_i + \frac{1}{2} [\xi_i]^T Q^i(z_i) [\xi_i]; \quad [\xi_i] = [x_i, y_i]^T \quad (3)$$

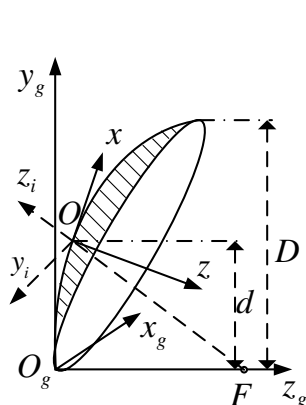


Figure 1. The offset reflector in the global coordinates system.

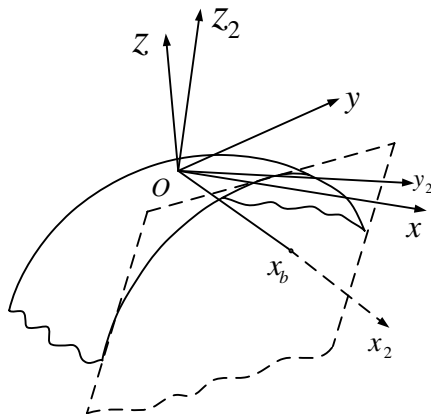


Figure 2. The reflecting surface containing a planar edge.

where (x_i, y_i, z_i) is the TD-GB incident coordinates system as shown in Fig. 1. More specifically as stated in [11].

3. FORMULATIONS OF THE STEP RESPONSE

In this section, the method in [11] is further improved to predict the characteristics of offset reflector. Step response formulations of offset reflector (or offset IRA) illuminated by TD-GB are presented. The coordinate transformation is used to simplify the step response to one dimensional angular integral which is independent of the reflector's size. These formulations are also available for parabolas of revolution.

The offset parabolic reflector, as shown in Fig. 1, is described in the global coordinates system (x_g, y_g, z_g) as

$$z_g = \frac{x_g^2 + y_g^2}{4F} \tag{4}$$

where F is the focal length of the reflector. Within amplitude taper distribution of TD-GB, the reflector can be approximated by a second order surface origin at O [14], where the TD-GB axis intersects the reflector. The second order surface expressed in the surface coordinates system (x, y, z) is

$$z(x, y) = -\frac{1}{2} \left(\frac{x^2}{R_1} + \frac{y^2}{R_2} \right) \tag{5}$$

where R_1 and R_2 are principal radius along x and y coordinates, as shown in Fig. 1.

The relationship between surfaces coordinates and incident TD-GB coordinates (x_i, y_i, z_i) can be expressed as [15]

$$\begin{bmatrix} x_i \\ y_i \\ z_i \end{bmatrix} = \begin{bmatrix} c_{11} & c_{12} & c_{13} \\ c_{21} & c_{22} & c_{23} \\ c_{31} & c_{32} & c_{33} \end{bmatrix} \begin{bmatrix} x \\ y \\ z \end{bmatrix} \quad (6)$$

To evaluate the surface integral which will be mentioned next, edge coordinates system is introduced. It is assumed that the x -axis of the edge coordinates system (x_2, y_2, z_2) is perpendicular to the plane containing the edge. The x -axis intersects the plane at $x_2 = x_b$, as shown in Fig. 2. The relationship between the surface coordinates system and edge coordinates system is expressed in matrix form [15]

$$\begin{bmatrix} x_2 \\ y_2 \\ z_2 \end{bmatrix} = \begin{bmatrix} b_{11} & b_{12} & b_{13} \\ b_{21} & b_{22} & b_{23} \\ b_{31} & b_{32} & b_{33} \end{bmatrix} \begin{bmatrix} x \\ y \\ z \end{bmatrix} \quad (7)$$

It should be noted that the three coordinates systems have the same origin at O where the incident TD-GB axis intersects the reflector.

As in [15], the projected area of the local parabolic surface S_a on the $z = 0$ plane in the surface coordinates system is shown in Fig. 3(a) and can be expressed as

$$\frac{(x - x_0)^2}{A^2} + \frac{(y - y_0)^2}{B^2} = d^2 \quad (8)$$

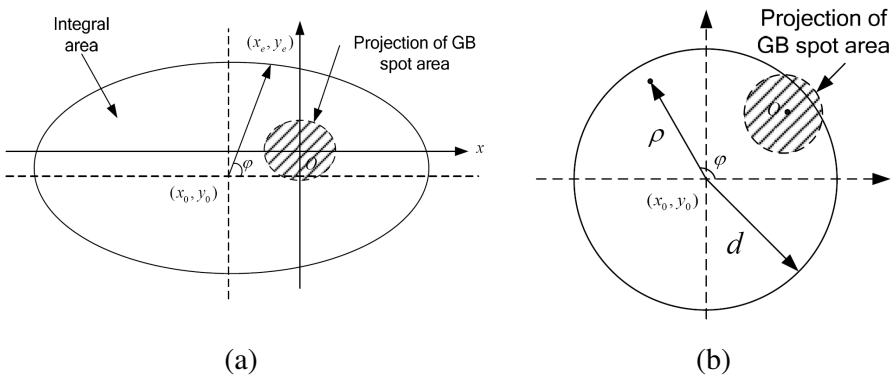


Figure 3. (a) The projected area of the local parabolic surface S_a on the $z = 0$ plane and (b) the local parabolic surface mapped to the (ρ, φ) coordinates system.

where

$$(x_0, y_0) = \left(\frac{b_{11}R_1}{b_{13}}, \frac{b_{12}R_2}{b_{13}} \right) \tag{9}$$

$$A^2 = \left| -\frac{2R_1}{b_{13}} \right|; \quad B^2 = \left| -\frac{2R_2}{b_{13}} \right|; \quad d^2 = \left| x_b - \frac{b_{11}^2R_1}{2b_{13}} - \frac{b_{12}^2R_2}{2b_{13}} \right| \tag{10}$$

Using the mapping

$$\begin{cases} x = x_0 + A\rho \cos \varphi \\ y = y_0 + B\rho \sin \varphi \end{cases} \tag{11}$$

The integral area can be transformed from Cartesian coordinates to polar coordinates as show in Fig. 3(b).

Next, the PO integral will be evaluated. As state in [11], the analytical step response is given as

$$\vec{E}_+^u(\vec{r}, t) \approx \frac{Z_0}{2\pi v r} \hat{r} \times \hat{r} \times \iint_{S_a} \hat{n} \delta_+ \left[t + \frac{f(x', y')}{v} \right] dS' \times \vec{H}_i^\delta(0) \tag{12}$$

where $Z_0 = 120\pi$ is the impedance of free space, S_a represents the reflector surface, $\vec{r} = (x, y, z)$ is the observation point and $\vec{r}' = (x', y', z')$ is the source point, \hat{n} is the unit vector normal to the surface at the source point \vec{r}' , $\vec{H}_i^\delta(0)$ is the value of GB at O , the complex phase term $f(x', y')$ is given in [15]

$$\begin{aligned} f(x', y') = R + q(\vec{r}_i) = & f(x_s, y_s) - a_0(x' - x_s)^2 - a_1(y' - y_s)^2 \\ & - 2c(x' - x_s)(y' - y_s) \end{aligned} \tag{13}$$

Let $\vec{P}_+(\vec{r}, t)$ represents the integral in (12)

$$\vec{P}_+(\vec{r}, t) = \frac{1}{v} \iint_{S_a} \hat{n} \delta_+ \left[t + \frac{f(x', y')}{v} \right] dS' \tag{14}$$

The calculation of this integral will be discussed in Appendix A. Actual physical responses are obtained by taking the real parts of these analytical responses. Impulse responses can be achieved by differentiating the step responses numerically.

4. NUMERICAL RESULTS AND DISCUSSION

In this section, TD scattered field of offset reflector is investigated and the FFT of the offset reflector’s impulse responses are compared to the direct FD result.

The complex curvature matrix $Q^i(z_i)$ in (1) is assumed to be

$$Q^i(z_i) = \begin{bmatrix} \frac{1}{z_i + jb_{11}} & 0 \\ 0 & \frac{1}{z_i + jb_{22}} \end{bmatrix} \quad (15)$$

For simplicity, $\vec{H}_i^\delta(0) = 1$ and the collimated distance $b_{11} = b_{22} = b = 1.0$ m are chosen. The diameter D of the offset reflector is 2.54 m, the focal length $F = 1.778$ m, and the offset distance d which measures from the z -axis of the global coordinates to the center of the offset reflector is 1.27 m, as shown in Fig. 1. The TD-GB waist is located at the focus point of offset reflector. The point where the beam axis intersects the surface is $(0, \frac{D}{2}, \frac{D^2}{16F})$ in the global coordinates system. The scattered field is observed at $(r \sin \theta \cos \varphi, r \sin \theta \sin \varphi, r \cos \theta)$ with $r = 100$ m in the global coordinates system.

Figure 4 shows step responses of the offset reflector for different observation angle θ with (a) for $\varphi = 0$ deg and (b) for $\varphi = 90$ deg. The peak values of the step responses are decreasing as the observation angle θ increased, because the reflector focuses the energy in its boresight direction. Compared with Fig. 4(a), step responses in Fig. 4(b) are moved forward as the observation angle increased, due to the unsymmetrical characteristics of the reflector in the $\varphi = 90$ deg plane.

Corresponding impulse responses are depicted in Figs. 5(a) and (b). It is shown that the TD impulse response just exhibits an impulsive behavior in the boresight direction, none in other directions. Peak values of these pulses decreased as the observation angle increased, which also implies the reflector focuses the energy in its boresight direction.

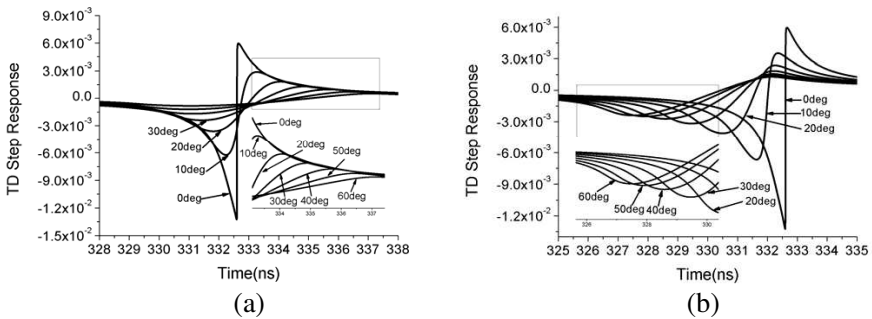


Figure 4. Step responses of offset parabolic reflector illuminated by a TD-GB (a) $\varphi = 0$ deg; (b) $\varphi = 90$ deg.

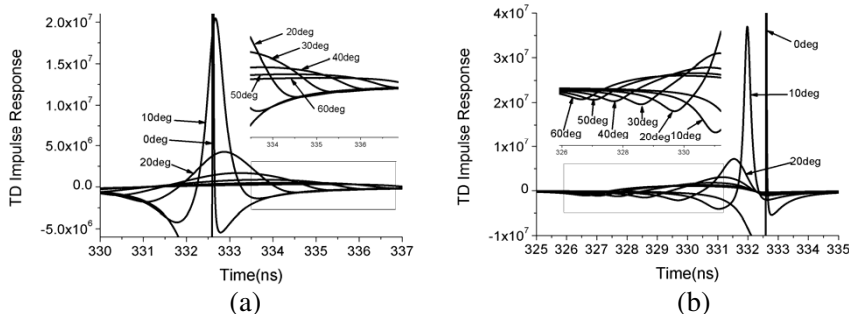


Figure 5. Impulse responses of offset parabolic reflector illuminated by a TD-GB (a) $\varphi = 0$ deg; (b) $\varphi = 90$ deg.

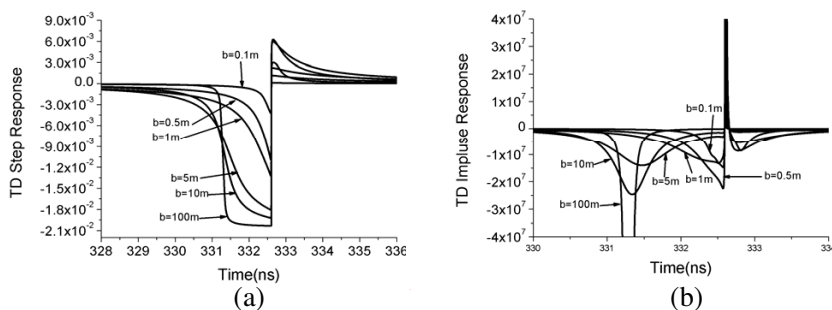


Figure 6. TD characteristics of offset parabolic reflector for various b . (a) Step responses; (b) Impulse responses.

To investigate the influence of parameter b on TD characteristics of the offset reflector, step responses at boresight direction with b changing from 0.1 m, to 100 m, are presented in Fig. 6(a). Corresponding impulse responses are shown in Fig. 6(b). For all values of b , an impulse is observed at 332.6 ns. Two impulsive pulses for $b = 100$ m are due to the fast decaying and rising of the rectangular pulse.

The FFT of impulse responses and direct FD result at 3.0 GHz are compared to validate this approach. The method state in [15] is chosen as FD method. The observation angle is ranging from -35 deg to 35 deg in θ direction with angular resolution of 1 deg. Both $\varphi = 0$ deg and $\varphi = 90$ deg are considered. Radiation patterns are listed in Fig. 7(a) for $\varphi = 0$ deg, and (b) for $\varphi = 90$ deg. The FFT of impulsive responses and direct FD result agree very well in the main beam. The discrepancy in wide angle is attributed to numerical errors in evaluating the angular

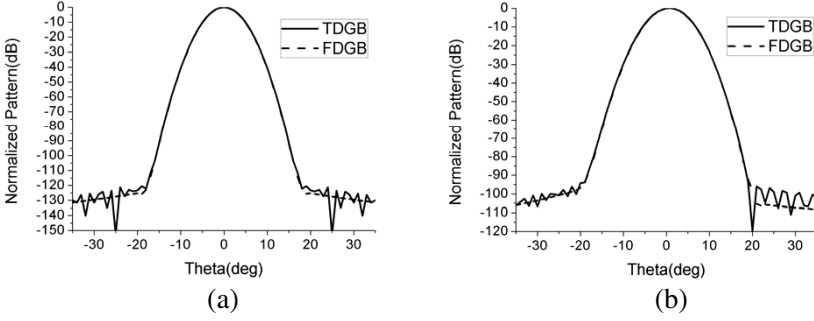


Figure 7. Comparison of TD and FD method at 3.0 GHz (a) $\varphi = 0$ deg; (b) $\varphi = 90$ deg.

integral. The effects of the numerical errors in this problem can be ignored since fields in Fig. 7 are about -100 dB less than the peak value, respectively. The unsymmetrical pattern in Fig. 7(b) contributes to the unsymmetrical characteristics of the offset reflector in $\varphi = 90$ deg plane.

5. CONCLUSION

In this paper, an improved transient quasi-analysis method for offset reflector is presented. Coordinate transformation is introduced to simplify the TD far-field integral to one dimensional angular integral. An investigation of the influences of observation angle as well as TD-GB collimated distance b on the step and impulse responses is also discussed. The FFT of impulse responses is compared with direct FD result, and good agreement is obtained. This method can also be easily extended to analyze radiation characteristics of offset IRAs illuminated by a variety of TD feed models, whose radiation field can be expanded to a set of TD-GBs.

APPENDIX A. EVALUATION OF $\vec{P}_+(\vec{R}, T)$ IN (14)

The unit vector \hat{n} normal to the offset reflector surface can be expressed as

$$\hat{n} = \frac{\hat{z} + \frac{x'}{R_1}\hat{x} + \frac{y'}{R_2}\hat{y}}{\sqrt{1 + \left(\frac{x'}{R_1}\right)^2 + \left(\frac{y'}{R_2}\right)^2}} \quad (\text{A1})$$

Using the mapping (11), the integral can be transformed from Cartesian coordinates to polar coordinates.

$$dS' = \sqrt{1 + \left(\frac{x'}{R_1}\right)^2 + \left(\frac{y'}{R_2}\right)^2} AB\rho d\rho d\varphi \tag{A2}$$

Using (A1) and (A2), (13) can be expressed as

$$\vec{P}_+(\vec{r}, t) = \frac{1}{v} \int_0^{2\pi} \int_0^d \left(\hat{z} + \frac{x'}{R_1} \hat{x} + \frac{y'}{R_2} \hat{y} \right) \delta_+ \left[t + \frac{f(x', y')}{v} \right] AB\rho d\rho d\varphi \tag{A3}$$

Using the mapping (11), $f(x', y')$ is expressed

$$f(x', y') = U\rho^2 + V\rho + W \tag{A4}$$

where

$$\begin{aligned} U &= -A^2 a_0 \cos^2(\varphi) - 2ABc \cos(\varphi) \sin(\varphi) - a_1 B^2 \sin^2(\varphi) \\ V &= -2Aa_0 x_0 \cos(\varphi) + 2Aa_0 x_s \cos(\varphi) - 2Acy_0 \cos(\varphi) \\ &\quad + 2Acy_s \cos(\varphi) - 2Bcx_0 \sin(\varphi) + 2Bcx_s \sin(\varphi) \\ &\quad - 2a_1 By_0 \sin(\varphi) + 2a_1 By_s \sin(\varphi) \end{aligned} \tag{A5}$$

$$\begin{aligned} W &= f(x_s, y_s) - a_0 x_0^2 + 2a_0 x_0 x_s - a_0 x_s^2 - 2cx_0 y_0 + 2cx_s y_0 \\ &\quad - a_1 y_0^2 + 2cx_0 y_s - 2cx_s y_s + 2a_1 y_0 y_s - a_1 y_s^2 \end{aligned}$$

Assuming $\rho_{1,2}$ are the two roots of $f(x', y') + vt = 0$, then

$$\rho_{1,2} = -(\rho_t \pm Q); \quad \rho_t = \frac{V}{2U}; \quad Q = \frac{\sqrt{V^2 - 4U(W + vt)}}{2U} \tag{A6}$$

So

$$\delta_+ \left[t + \frac{f(x', y')}{v} \right] = \frac{jv}{U\pi(\rho - \rho_1)(\rho - \rho_2)} \tag{A7}$$

Using (A7), (A3) can be expressed as

$$\vec{P}_+(\vec{r}, t) = \int_0^{2\pi} \int_0^d \left(\hat{z} + \frac{x'}{R_1} \hat{x} + \frac{y'}{R_2} \hat{y} \right) \frac{j}{U\pi(\rho - \rho_1)(\rho - \rho_2)} AB\rho d\rho d\varphi \tag{A8}$$

Let

$$\vec{P}_+(\varphi) = \int_0^d \left(\hat{z} + \frac{x'}{R_1} \hat{x} + \frac{y'}{R_2} \hat{y} \right) \frac{j}{U\pi(\rho - \rho_1)(\rho - \rho_2)} AB\rho d\rho \tag{A9}$$

Express $\vec{P}_+(\varphi)$ in x, y and z components, we can get

$$\vec{P}_+(\varphi) = \hat{x}P_+^x(\varphi) + \hat{y}P_+^y(\varphi) + \hat{z}P_+^z(\varphi) \tag{A10}$$

where

$$\vec{P}_+^x(\varphi) = \frac{jAB}{U\pi R_1} \left[x_0 \int_0^d \frac{\rho}{(\rho - \rho_1)(\rho - \rho_2)} d\rho + A \cos(\varphi) \int_0^d \frac{\rho^2}{(\rho - \rho_1)(\rho - \rho_2)} d\rho \right] \quad (\text{A11})$$

$$\vec{P}_+^y(\varphi) = \frac{jAB}{U\pi R_1} \left[y_0 \int_0^d \frac{\rho}{(\rho - \rho_1)(\rho - \rho_2)} d\rho + B \sin(\varphi) \int_0^d \frac{\rho^2}{(\rho - \rho_1)(\rho - \rho_2)} d\rho \right] \quad (\text{A12})$$

$$\vec{P}_+^z(\varphi) = \frac{jAB}{U\pi} \int_0^d \frac{\rho}{(\rho - \rho_1)(\rho - \rho_2)} d\rho \quad (\text{A13})$$

The integral with ρ can be calculated with the following relationships

$$\int_0^d \frac{\rho}{(\rho - \rho_1)(\rho - \rho_2)} d\rho = \frac{1}{2Q} \left[-\rho_1 \ln \frac{\rho_1 - d}{\rho_1} + \rho_2 \ln \frac{\rho_2 - d}{\rho_2} \right] \quad (\text{A14})$$

$$\int_0^d \frac{\rho^2}{(\rho - \rho_1)(\rho - \rho_2)} d\rho = \frac{1}{2Q} \left[2Qd - \rho_1^2 \ln \frac{\rho_1 - d}{\rho_1} + \rho_2^2 \ln \frac{\rho_2 - d}{\rho_2} \right] \quad (\text{A15})$$

The integral of ρ in (A3) is calculated in closed form and the integral of φ which is independent of the reflector size is calculated in numerical form.

ACKNOWLEDGMENT

This work was supported by the postdoctoral Science Foundation of China (No. 20090461325, No. 201003690), the National Natural Science Foundation of China (No. 61001029, No. 10876007), the Fundamental Research Funds for the Central Universities (No. ZYGX2010X005).

REFERENCES

1. Baum, C. E., "Radiation of impulse-like transient fields," *Sensor and Simulation Note 321*, Weapons Laboratory, Nov. 25, 1989.
2. McLean, J. S., R. Sutton, and H. Foltz, "The minimum phase nature of the transfer function of the impulse radiating antenna," *PIERS Online*, Vol. 7, No. 4, 380–386, 2011.
3. Bajracharya, C., S. Xiao, C. E. Baum, and K. H. Schoenbach, "Target detection with impulse radiating antenna," *IEEE Antenna and Wireless Propagation Letters*, Vol. 10, 496–499, 2011.

4. Kim, K. and W. R. Scott, "Impulse-radiating antenna with an offset geometry," *IEEE Trans. Antennas and Propagat.*, Vol. 53, 1738–1744, 2005.
5. Li, J., L.-X. Guo, and H. Zeng, "FDTD method investigation on the polarimetric scattering from 2-d rough surface," *Progress In Electromagnetics Research*, Vol. 101, 173–188, 2010.
6. Zhang, G. H., M. Xia, and X. M. Jiang, "Transient analysis of wire structures using time domain integral equation method with exact matrix elements," *Progress In Electromagnetics Research*, Vol. 92, 281–298, 2009.
7. Sun, E.-Y. and W. V. T. Rusch, "Time-domain physical-optics," *IEEE Trans. Antennas and Propagat.*, Vol. 42, 9–15, 1994.
8. Johansen, P. M., "Time-domain version of the physical theory of diffraction," *IEEE Trans. Antennas and Propagat.*, Vol. 47, 261–270, 1999.
9. Rousseau, P. R., P. H. Pathak, and H.-T. Chou, "A time domain formulation of the uniform geometrical theory of diffraction for scattering from a smooth convex surface," *IEEE Trans. Antennas and Propagat.*, Vol. 55, 1522–1534, 2007.
10. Heyman, E., "Pulsed beam propagation in inhomogeneous medium," *IEEE Trans. Antennas and Propagat.*, Vol. 42, 311–319, 1994.
11. Chou, H.-T., S.-C. Tuan, and H.-H. Chou, "Transient analysis of scattering from a perfectly conducting parabolic reflector illuminated by a gaussian beam electromagnetic field," *IEEE Trans. Antennas and Propagat.*, Vol. 58, 1711–1719, 2010.
12. Tuan, S.-C. and H.-T. Chou, "Analytical solutions of TD scattering fields from parabolic reflector antenna illuminated by plane waves and gaussian beams," *PIERS Proceedings*, 1467–1470, Xian, China, Mar. 22–26, 2010.
13. Rousseau, P. R., "Time domain version of the uniform geometrical theory of diffraction," Ph.D. Dissertation, ElectroScience Lab., The Ohio State University, Columbus, 1995.
14. Chou, H.-T., P. H. Pathak, and R. J. Burkholder, "Novel Gaussian beam method for the rapid analysis of large reflector antennas," *IEEE Trans. Antennas and Propagat.*, Vol. 49, 880–893, 2001.
15. Chou, H.-T. and P. H. Pathak, "Uniform asymptotic solution for the EM reflection and diffraction of an arbitrary Gaussian beam by a smooth surface with an edge," *Radio Sci.*, Vol. 32, 1319–1336, 1997.